Numerical analysis of the elastic-plastic behavior of a tubular structure in FGM under pressure and defect presence

A. Houari, A.S. Bouchikhi
Department of mechanical Engineering, Laboratory – LMSS. BP 89, Sidi Bel-Abbes, Algeria
amingenie14@gmail.com, asbouchikhi@yahoo.fr

M. Mokhtari
Ecole Nationale Polytechnique Maurice Audin, Oran 31000, Algeria
mohamed.mokhtari@enp-oran.dz

K. Madani
Department of mechanical Laboratory LMPM, Sidi Bel Abbes 22000, Alegria
koumad10@yahoo.fr

ABSTRACT. Given the field of application and the many advantages, the use of FGM (Functionally Graded Materials) has recently been extended in several components and more particularly in cylindrical structures, which have been the subject of several recent studies. Our work aims to use the finite element method to analyze a cylindrical structure in FGM with properties gradated in the direction of the radius (Thickness) solicited purely in internal pressure by the implementation of a UMAT subroutine in the calculation code ABAQUS. The elasto-plastic behavior of the FGM is described by the flow theory represented by the equivalent stress of Von Mises and an incremental hardening variable. The TTO model (Tamura-Tomota-Ozawa) was used only to determine the elastic-plastic properties of the FGM. The radial, tangential and axial stresses according to the thickness were evaluated in the first part of our work. In the second part, these stresses are evaluated under the same conditions but with the presence of a micro-cavity. The results obtained show clearly that these stresses are in direct relation not only with the thickness and properties of the FGM tube but also with the presence of the cavity.

KEYWORDS. FGM (Functional Graded Materials); UMAT (User Materials); Defect (Closed pores).

INTRODUCTION

With industrial development, pressure vessels and tubes are widely used in reactor technology, chemical industries, marine engineering and aerospace. Since in most applications the vessels must operate under extreme thermal and mechanical loads, any failure or fracture will be an irreparable disaster. Consideration of

the strength of these components is therefore very important to ensure a long service life.

FGMs represent a new generation of composite materials because of their many advantages. The most important feature of FGMs is the variable and continuous distribution of the material, which is advantageous for their application under adverse conditions such as high temperatures and pressures, excessive wear and corrosion while maintaining their structural properties, machinability and thermal conductivity. These FGMs have been fabricated using many techniques including gas, liquid, and solid phase methods [1]. Processes such as centrifugal casting, sedimentation casting, directional solidification, and infiltration processing are the popular processing methods generally employed [2].

The gradation of the two materials can be controlled by selected laws such as the power law (volume fraction law) and the law of exponentials (Ghannad and Gharooni [3], Durmus and Keles [4])). Thick cylinders as structures are the subject of our study which are used in various industrial fields. The analysis of these structures under internal pressure and by the presence of defects, such as micro-cavities, which generate a high stress concentration which can become important if the structure, is subjected to high stress.

Several studies have focused on the analysis of cylindrical FGM structures such as (Tounsi and Bedia [5], Wu and Liu [6], Bich and Tran [7]) which have analyzed the effect of the gradation of a cylindrical FGM structure depending on the thickness. Kordkheili et al [8] and Safari et al [9] presented a solution by an analytical method for the mechanical behavior of a cylindrical structure in FGM, while Sharma et al [10] and You et al [11] consider in their analysis a purely elastic behavior on a spherical structure under internal pressure. Similarly, the work of Foroutan et al [12] present in their static analysis of FGM cylinders subjected to internal and external pressure, a method without mesh. They assumed that the mechanical properties of the cylinders were variable in the radial direction and consider that the results obtained for these cylinders were compared to the analytical solutions and a very good agreement was observed between them. While some researchers (Ghannad and Nejad [13], Eraslan [14], Ghannad et al [15], Chen [16]) have invested in the analysis of cylinders under non-uniform internal pressure, others like Bayat et al [17] and Carrera et al [18] analyzed the mechanical behavior of tubular structures in FGM using the analytical and numerical method under transverse load. On the other hand, other studies (Cinefra and Belouettar [19], Houari and Tounsi [20], Otbi and Bedia [21], Barka, and Tounsi [22]) introduce the effect of thermo-mechanical loading on the response of a thick plate in FGM. Kaci et al [23] analyzed the nonlinear bending behavior of a cylindrical structure with exponential functional gradation (simply called E-FG) of variable thickness; they assume that the material properties of functionally graduated plates, at the except the Poisson's ratio, vary continuously on the thickness of the plate according to the exponential law of distribution. Kerimcan et al [24] have used the method of complementary functions (CFM) to determine the thermal and mechanical stresses in one-dimensional steady state for different values of constant of inhomogeneity in a thick hollow sphere in functionally graded material (FGM) where they assumed that the mechanical properties obey exponential variations in the radial direction. Sharma et al [25] and Wang et al [26] used the finite element method to analyze the response of an FGM structure subjected to a combined stress of torsion and internal and external pressure.

The plasticity of the metal plays a major role in the behavior of the FGM. Several researchers have shown their interest in this area as Praveen and Reddy [27]. A large part of the studies on the elasto-plastic behavior on FGM cylinders has been carried out numerically, namely the work of Horgan et al [28] and Figueredo et al [29] who have proposed a numerical methodology to predict the behavior of elastic stress -plastic functionally graded cylindrical vessels subjected to internal pressure. For the nonlinear analysis of the FGM, the work of Trabelsi et al [30] and Kar et al [31-32] is devoted to the use of the Shell element in the modeling of structures under different types of stresses as well as on nonlinear thermal analyzes of FGM structures under different types of mechanical and thermal stresses. While Hanen et al [33] use the extended finite element method to analyze both geometrical and material nonlinear behavior of general plate-shell type structures in functionally classified material, Amir et al [34]   proposes a new solution of elasto-plastic stress in axisymmetric problems (rotating disc, cylindrical and spherical vessel). The study of nonlinear vibrations in FGM was the basis of the research of Kutlu [35] and Hadji et al [36]). Recently Khalid et al [37] implemented a UMAT in the code of ABAQUS to study the flexion and the free vibration of the plate in FGM.

Other research, using the finite element method, have analyzed the effect of porosity in the analysis of inter-facial stresses of FGM beams perfectly reinforced with a plate of porous materials with functional gradation, whereas Benferhat et al [38-39] studied the effect of shapes and the distribution of porosity on the bending behavior of a plate in FGM and developed a general model to predict the distribution of the interfacial shear stress and the normal stresses of the beam (FG) reinforced by porous FGM plates under mechanical loading. They showed that the normal and shear stresses at the interface are influenced by the material parameters and that the inhomogeneities play an important role in the distribution of these interfacial stresses.

Therefore, they have shown that functionally graded panel reinforcement systems in the presence of porosity are effective in improving the bending behavior of reinforced FGM beams. Benferhat et al [39] proposed a modification of the mixing

law to describe an approximation on the material properties of FGM plates with porosity phases. Nguyen et al [40] analyzed the behavior of the porous FGM and they assumed two different porosity distributions according to the direction of the thickness (regular and unequal) while Jae-Chul [41] concluded that the distribution of porosity in the cylinder in FGM is nonlinear. We also cite other analyses on FGMs by introducing the porosity effect such as the work of (Benferhat et al [39]).

The work of Bekki et al [42] aims to study the effect of the shapes of the porosity distribution on the bending behavior of the simply supported FG plate; they developed a refined theory of shear deformation to study the effect of the shape of the porosity distribution on the static behavior of FGM plates. It has been found that the shape of the porosity distribution significantly influences the mechanical behavior of FGM plates in terms of deformation and normal and shear stresses.

Our work fits within this context; we aim to analyze, by the finite element method using the Abaqus code, the variation of circumferential, radial and axial stresses in a tubular structure in FGM. The material of the cylinder is assumed to be isotropic and heterogeneous, sollicited only under internal pressure, its mechanical properties vary radially along the thickness according a power function; the elasticity modulus and the Poisson's ratio are variable. In the first part of our analysis, the variation of the different stresses is presented as a function of the relationship between the outside and inside diameters as well as the gradation exponent "n". In the second part, we assume the presence of defects (cavity) in different positions in the FGM, the axial and radial stresses were evaluated under these different effects.

FORMULATION OF THE PROBLEM

In our work, we consider a thick axisymmetric cylinder in non-homogeneous FGMs subjected to a uniform pressure on the interior surface. Let us take an element of infinitely small volume, see Fig.1 (a):

(a) Cylindrical representation of the stresses,

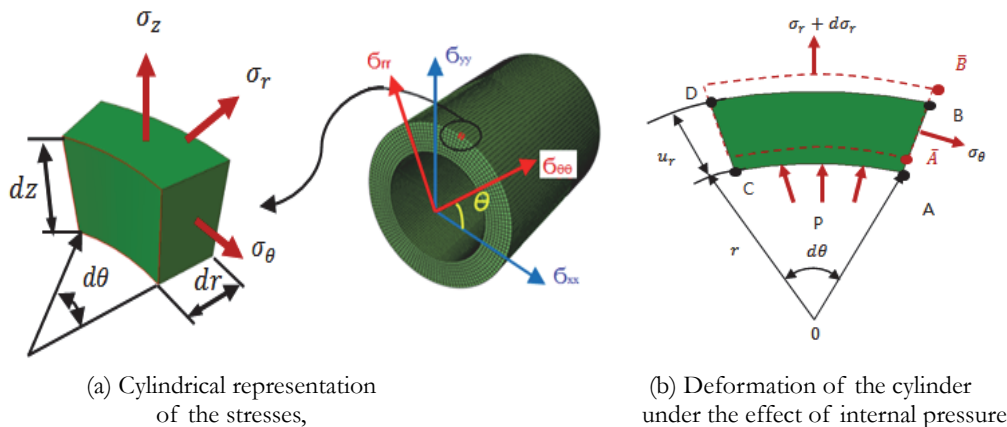(b) Deformation of the cylinder under the effect of internal pressure

Figure 1: Cylindrical presentation.

The linear relation between the stresses and strains is given by the Hook's law. In order to implement a UMAT subroutine in the ABAQUS calculation code in the form of a numerical algorithm, it is necessary to use the elasticity relation isotropic in three dimensions given by the expression:

$$\sigma_{ij} = \lambda(r)\delta_{ij}\varepsilon_{kk} + 2G(r)\varepsilon_{ij} \tag{1}$$

σ_{ij} : is the true stress in the material, ε_{ij} the strain tensor, δ_{ij} the Kronecker delta.

Where the two Lame coefficients: $\lambda(r)$ and $G(r)$ are expressed as a function of the Young's modulus $E(r)$ and the Poisson's ratio $v(r)$ which are continuously graded by the coordinates (r,θ,z) in the UMAT:

$$\lambda(r) = \frac{E(r)}{(1+v(r))(1+2v(r))} \quad \text{and} \quad G(r) = \frac{E(r)}{2(1+v(r))} \tag{2}$$

Under the effect of pressure the internal diameter increases, giving rise to the radial stresses σ_r and tangential σ_θ (Fig. 1(b)), after deformation, A moves in A' and B in B'. From the geometric relations in Fig.1, we have:

$$\varepsilon_r(r) = du(r)/dr \, , \ \varepsilon_\theta(r) = u(r)/r \, , \ \varepsilon_z(r) = dw_z/dz \ \text{ and } \ \varepsilon_r(r) = \varepsilon_\theta(r) + r\frac{d\varepsilon_\theta(r)}{dr} \tag{3}$$

The components of the tensor of the Cauchy stresses are as follows:

$$\sigma_r(r) = \frac{E(r)}{1+v^2(r)}\Big[\varepsilon_r(r) + v(r)\varepsilon_\theta(r)\Big] \tag{4.a}$$

$$\sigma_\theta(r) = \frac{E(r)}{1+v^2(r)}\Big[\varepsilon_\theta(r) + v(r)\varepsilon_r(r)\Big] \tag{4.b}$$

$$\sigma_z(r) = v(r)\Big[\varepsilon_r(r) + \varepsilon_\theta(r)\Big] \tag{4.c}$$

where $\sigma_r(r)$, $\sigma_\theta(r)$ and $\sigma_z(r)$ are the radial, circumferential, and axial stresses, respectively, as a function of (r), $\varepsilon_r(r)$ and $\varepsilon_\theta(r)$ are the radial and circumferential strain, respectively, as a function of (r), while ε_z is the axial strain and is assumed to be constant, taking the large length-radius ratio into consideration, and whereas $u(r)$ is the radial displacement as a function of (r) and $w(z)$ is the axial displacement as function of length. $v(r)$ is the poison's ratio. According to the infinitesimal strain theory, the equilibrium equation and the strain displacement relations for an axisymmetric structure can be written, respectively, as:

$$\frac{d\sigma_r(r)}{dr} + \frac{\sigma_r(r) - \sigma_\theta(r)}{r} = 0 \tag{5}$$

In our analysis, the elastic-plastic behavior of a metal matrix FGM reinforced with ceramic particles is described with a flow surface represented by an equivalent Von Mises stress and an isotropic hardening variable of our FGM. The hardening subroutine (UHARD) is used to check whether the material has undergone plastic deformation. The total deformation $\varepsilon(r)$ in the corotational coordinate system of an FGM as in all elastic-plastic materials has a reversible elastic part $\varepsilon^e(r)$ and an irreversible plastic part $\varepsilon^p(r)$, according to the next equation:

$$\varepsilon_r(r) = \varepsilon_r^p(r) + \varepsilon_r^e(r) \tag{6.a}$$

$$\varepsilon_\theta(r) = \varepsilon_\theta^p(r) + \varepsilon_\theta^e(r) \tag{6.b}$$

$$\varepsilon_z(r) = \varepsilon_z^p(r) + \varepsilon_z^e(r) \tag{6.c}$$

By replacing respectively the Eqns. (4) in Eqns. (6):

$$\varepsilon_r(r) = \varepsilon_r^p(r) + \tfrac{1}{E(r)}\big(\sigma_r(r) - v(r).\sigma_\theta(r)\big) \tag{7}$$

$$\varepsilon_\theta(r) = \varepsilon_r^p(r) + \tfrac{1}{E(r)}\big(\sigma_\theta(r) - v(r).\sigma_r(r)\big) \tag{8}$$

The relation between the stresses and the plastic strains is determined from subtraction the Eqns. (7) and (8):

$$\varepsilon_r^p(r) - \varepsilon_\theta^p(r) + r\frac{d\varepsilon_\theta^p(r)}{dr} = \frac{1}{E(r)}\left(\frac{d\sigma_\theta(r)}{dr} + \frac{d\sigma_r(r)}{dr}\right) - \frac{r}{E^2(r)}\frac{dE(r)}{dr}\left(\sigma_\theta(r) - v(r).\sigma_r(r)\right) \tag{9}$$

To solve this differential equation, one uses the criterion of plasticity determined by the flow surface and is given according to the criterion of Von Mises by:

$$f(\sigma,R) = \sigma_{eq} - \sigma_r = 0 \tag{10}$$

$f(\sigma,R)$: is the yield function, σ_{eq}: is the equivalent stress Von Mises of FGM and σ_r: represents the radius of the yield surface. If $f(\sigma,R)$ is negative then the behavior of the material is elastic, if not $f(\sigma,R)$ remains zero, there will be plastic flow. From Eqn. (11), we define the equivalent Von Mises stress σ_{eq} and the deviator (S) by:

$$\sigma_{eq} = \sqrt{\frac{2}{3}S.S} \ , \ \sigma_{eq} = \frac{1}{\sqrt{2}}\sqrt{\left(\sigma_\theta - \sigma_r\right)^2 + \left(\sigma_\theta - \sigma_z\right)^2 + \left(\sigma_r - \sigma_z\right)^2} \tag{11}$$

$$S = \begin{bmatrix} S_r \\ S_\theta \\ S_z \end{bmatrix} = \begin{bmatrix} \dfrac{2\sigma_r - \sigma_\theta - \sigma_z}{3} \\ \dfrac{2\sigma_\theta - \sigma_r - \sigma_z}{3} \\ \dfrac{2\sigma_z - \sigma_r - \sigma_\theta}{3} \end{bmatrix} \tag{12}$$

The evolution of the plastic strain $d\varepsilon^p$ is governed by a normal flow law of the plasticity criterion:

$$d\varepsilon^p = d\lambda\frac{\partial f}{\partial\sigma} = d\overline{\varepsilon}^p N, N = \frac{\partial f}{\partial\sigma} = \frac{2S}{3\sigma_{eq}} \tag{13}$$

As a function of the tensor de^p , the term $d\overline{\varepsilon}^p$ can be written as follows:

$$dp = d\overline{\varepsilon}^p = \sqrt{\frac{3}{2}de^p de^p} \tag{14}$$

where N is the gradient of the yield function with respect to the stress tensor, $d\overline{\varepsilon}^p$ is the (scalar) equivalent plastic strain rate. The isotropic hardening function $\sigma(r)$ of the FGM will be described as:

$$\sigma(r) = \sigma_{y0}(r) + R(p) \ \text{ and } \ R(p) = H.p \tag{15}$$

where $\sigma_{y0}(r)$ is the initial yield stress of the FGM and $R(p)$ is the isotropic hardening. To obtain the plastic multiplier $d\lambda$, it is therefore sufficient to express the law of evolution of the variable $R(p)$ as a function of the flow variables.
Using the Prandtl-Reuss law to determine the evolution of the variable in our case in uniaxial tension, the equality $f(\sigma,R) = 0$ can be summed up in the form:

$$\sigma(r) = \sigma_{y0}(r) + R(\varepsilon^p) \ \text{ and } \ H = \frac{R(\varepsilon^p)}{d\varepsilon^p} \tag{16}$$

where H is the hardening modulus of FGM and $d\varepsilon^p$ is the plastic strain rate, the plastic multiplier can then be easily proven to be equal to the rate of the accumulated plastic strain, using Eqns. (13), (14) and Eqn.(12):

$$dp = \sqrt{\frac{2}{3}\left(\frac{3d\lambda}{2}\frac{S}{\sigma_{eq}}\right)\left(\frac{3d\lambda}{2}\frac{S}{\sigma_{eq}}\right)} = \sqrt{\frac{2}{3}d\lambda^2\frac{S}{\sigma_{eq}}\frac{S}{\sigma_{eq}}} \quad dp = d\lambda \quad \text{and} \quad dp : \text{is the plastic multiplier} \tag{17}$$

The plastic multiplier $d\overline{\varepsilon}^p$ in Eqn.(14) is determined by using the consistency condition, which leads to:

$$\frac{\partial f}{\partial \sigma}\dot{\sigma} + \frac{\partial f}{\partial R}\dot{R} = 0 \quad \text{and} \quad \dot{R} = \frac{\partial R}{\partial p}\dot{p} \tag{18}$$

and making use of Eqn.(18) and Eqn.(14) along with substitutions, we obtain the following expression for the plastic multiplier $d\lambda = dp$:

$$d\lambda = d\overline{\varepsilon} = \frac{N:C:d\varepsilon}{N:C:N+H} \tag{19}$$

At the end, Prandtl-Reuss law makes possible to determine the 3D expression of the plastic strain rate, in the form:

$$d\varepsilon^p = d\lambda N = \frac{N:C:d\varepsilon}{N:C:N+H} \tag{20}$$

To solve Eqn.(20) we use the 'Backward Euler' integral method, Eqn.(13), gives:

$$\Delta\varepsilon^p = \Delta\overline{\varepsilon}^p N \tag{21}$$

Combining this with the deviatoric elasticity Eqn. (11) and the integrated strain rate decomposition Eqn. (21) gives:

$$S = 2G(\hat{\varepsilon} - \Delta\overline{\varepsilon}^p N) \quad \text{Where:} \quad \hat{\varepsilon} = \varepsilon^e - \Delta\varepsilon \tag{22}$$

$\Delta\varepsilon$: is the new total strain increment. Thereafter using the integrated flow rule Eqn.(13), together with the Von Mises definition of the flow direction, (in Eqn. 22), this becomes:

$$S\left(1 + \frac{3G}{\sigma_{eq}}\Delta\overline{\varepsilon}^p\right) = 2G\hat{\varepsilon} \tag{23}$$

The product of Eqn.(23) with itself gives us Newton's nonlinear equation:

$$\overline{\sigma}\left(\overline{\varepsilon}^p\right) = 2G\varepsilon^p_{eq} - 3G\Delta\lambda \tag{24}$$

The term $2G\varepsilon^p_{eq}$ represent the value of σ_{eq} at the start of each step and $\overline{\sigma}(\overline{\varepsilon}^p)$: is the new stress which must verify the uniaxial relation. We solve Eqn.(24) by Newton's method:

$$\Delta\lambda = \frac{\overline{\sigma}(\overline{\varepsilon}^p) - \sigma_{eq} + 3G\Delta\overline{\varepsilon}^p}{3G + H} = \frac{f}{3G + H} \quad \text{where} \quad H = \frac{d\overline{\sigma}(\overline{\varepsilon}^p)}{\Delta\overline{\varepsilon}^p} \tag{25}$$

$$\Delta \bar{\varepsilon}^{p} = \Delta \bar{\varepsilon}^{p} + \Delta \lambda \tag{26}$$

where, H is the hardening modulus recalculated at the end of each iteration. By substituting Eqn.(26) into Eqn.(1) one obtains:

$$d\sigma = C(d\varepsilon - \Delta \bar{\varepsilon}^{p}.N) \tag{27}$$

We can obtain the complete elasto-plastic incremental stress-strain relation:

$$d\sigma = C^{ep} d\varepsilon \quad \text{and} \quad C^{ep} = C - \frac{9G^{2} S.S}{(3G+H)\sigma_{eq}^{2}} \tag{28}$$

C^{ep} :is the fourth –order tensor known as the elasto-plastic tangent operator. Finally the new stresses (σ) at the end of the time step (Δt) can then be written as:

$$\sigma_{t+1} = \sigma_{t} + d\sigma \tag{29}$$

The index $(t+1)$ denotes the values at the end of the time increment. In the TTO (Tamura-Tomota-Ozawa) model (Carpenter et al [43]), the mixture of materials is treated as elasto-plastic with isotropic linear hardening, for which the stresses and deformations are related to the constituent efforts σ_{m}, σ_{c} and $\varepsilon_{m}, \varepsilon_{c}$:

$$\sigma = \sigma_{m} V_{m} + \sigma_{c} V_{c} \tag{30}$$

$$\varepsilon = \varepsilon_{m} V_{m} + \varepsilon_{c} V_{c} \tag{31}$$

where the subscripts c and m indicate the ceramic and metal, respectively.
The volume fraction of metal is denoted by V_{m}, Where: σ_{m}, σ_{c} and $\varepsilon_{m}, \varepsilon_{c}$: are the average stresses and strains in metal and ceramic, respectively. In the TTO model an additional parameter (q) is introduced which represents the ratio of stress to strain transfer, note that:

$$q = (\sigma_{c} - \sigma_{m}) / (\varepsilon_{c} - \varepsilon_{m}) \ , \ 0 \le q \le \infty \tag{32}$$

We are interested here mainly in the plastic part, the properties of the FGMs are described by the following relations:

$$E(r) = \left[\frac{q+E_{c}}{q+E_{m}} E_{m} V_{m} + E_{c} (1-V_{m}) \right] / \left[\frac{q+E_{c}}{q+H_{m}} V_{m} + (1-V_{m}) \right] \tag{33}$$

$$\sigma_{Y}(r) = \left[\frac{q+E_{m}}{q+E_{c}} \frac{E_{c}}{E_{m}} (1-V_{m}) + V_{m} \right] \sigma_{m} \tag{34}$$

$$H(r) = \left[\frac{q+E_{c}}{q+H_{m}} H_{m} V_{m} + E_{c} (1-V_{m}) \right] / \left[\frac{q+E_{c}}{q+H_{m}} V_{m} + (1-V_{m}) \right] \tag{35}$$

where $E(r)$ is the Young's modulus of the composite FGM. $\sigma_{Y}(r)$ is the yield stress of the FGM. The poison's ratio $v(r)$ of the composite just follows a rule of mixtures in the TTO model:

$$v(r) = v_m V_m + v_c V_c \tag{36}$$

The empirical parameter (q) depends on many factors including material composition, microstructural arrangement, and internal stresses. In our analysis, it is assumed that the elasto-plastic behavior of the FGM cylinder in ceramic matrix reinforced by ceramic particles varies continuously over the entire thickness of radius (r). In the inner radius R_{in} the metal distribution $V_m = 0$ and in the outer radius R_{ex} the metal fraction $V_m = 1$ a function of the volume fraction of the constituent materials, according to the following ratio:

$$V_m = \left(r - R_{in} / R_{ex} - R_{in} \right)^n \tag{37}$$

V_m is the volume fraction of metal, (r) is the tube thickness and (n) is an exponent of the volume fraction that adjusts the variation of the material profile across the thickness of the FGM layer. Using MATLAB, we find that the distribution of elasticity modulus along the radius by the power law of $n = 0.65$ see Fig.2, is similar to that of the exponential law. Remember that the expression of the exponential distribution is given by:

$$E(r) = E_m e^{\beta \cdot r} \quad \text{and} \quad \beta = \frac{1}{\left(R_{ex} - R_{in} \right)} \log \frac{E_c}{E_m} \tag{38}$$

where $E(r)$ is the Young's modulus of the FGM, E_m is the Young's modulus of the metal and Ec is the Young's modulus of the ceramic.

The elastic properties of ceramic-metal FGM are chosen from the work of Kalali and al [44], are listed in Tab. (1).

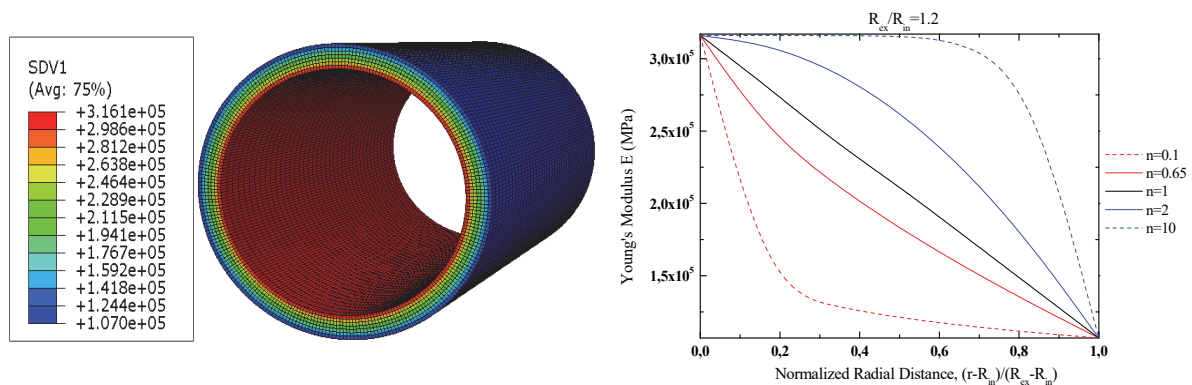|	Ceramic TiB	Metal Ti [43]
Young's modulus	E = 316000 MPa	E = 107000 MPa
Poison's ratio	ν = 0.17	ν = 0.34
Yield stress	-	σ_{y0} = 450 MPa
Hardening modulus	-	H = 10000 MPa

Table 1: The main mechanical properties.

Figure 2: Variation of the Young's Modulus of the power Law (image defined for the gradation exponent n = 1 with STATEV1).

The parameter « q » may be approximated by calibration of experimental data from tensile test performed on monolithic composite specimens. For example, a value of q=4500 MPa is used for a TiB/Ti composite.
The choice of Titanium boride at room temperature (TiB) as reinforcement in monolithic Ti-MMCs has several distinct

advantages over other possible titanium (Ti) compounds; there is a dramatic increase in strength when TiB whiskers are added to Ti by itself. [45].

DESCRIPTION OF MODEL GEOMETRY

T he geometries of the tubular structure with these standardized dimensions are illustrated in Fig.3. Its mechanical characteristics are quoted in Tab. (1). The ceramic was graded in the metal according to the thickness of the inner R_{in} outward R_{ex} by the choice of three different cases: by the fixed inner radius dimension of $R_{in} = 50$ mm and varying the outside $R_{ex} = 55, 60$ and 65mm , making a ratio of $R_{ex} / R_{in} = 1.1$, $R_{ex} / R_{in} = 1.2$ and $R_{ex} / R_{in} = 1.3$. The length of the cylinder is L=200 mm is sufficient to ensure that no stress interference exists in the region from the ends. This length of the cylinder should only act as a means of attachment to limit only the pressure effect on the micro-cavity presence of our studied FGM structure.
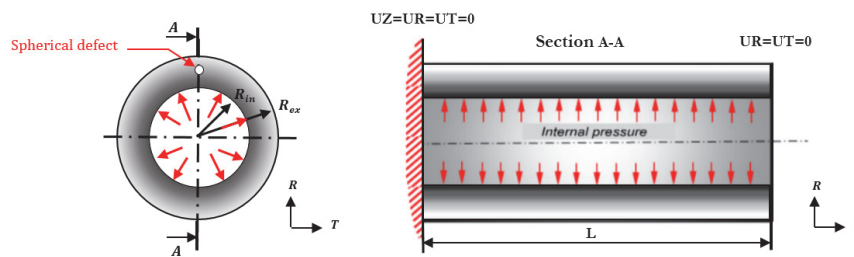

Figure 3: Overview of the studied geometry.

The numerical analysis of the behavior of the tubular structure was evaluated under the effect of internal pressure. The shape of the cavity is considered a spherical defect of dimension 0.5 mm taken for each location in the FGM and for each variation in the geometric ratio R_{ex} / R_{in} and the gradation exponent. The micro-cavity was positioned in the middle of the pipe length and along the radius in: a) near inside diameter (ceramic), b) in the middle of the thickness and c) near the outside diameter (metal), see Fig.4.
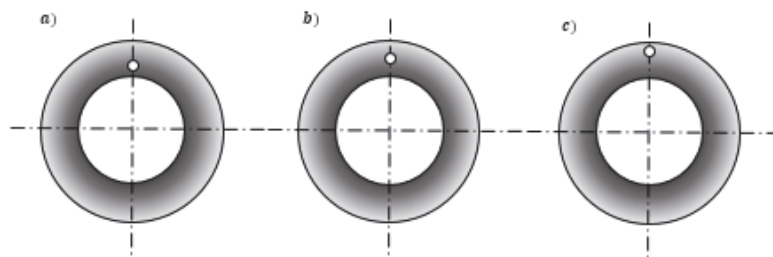

Figure 4: Spherical micro-cavity position according to the thickness of pipes in FGM.

Since the elasto-plastic behavior of the metal was introduced into the FGM, the internal pressure level was chosen at 100 MPa in order to cause plasticization in the cavity and in particular when the defect moves away from the ceramic part of the cylinder (outside diameter). For all the situations studied, the loading conditions are as follows: fasteners applied to the ends of one side, the three directions $\left(U_R = U_\theta = U_Z = 0 \right)$ and on the other side only the two directions $\left(U_R = U_\theta = 0 \right)$ to release the deformation in the direction U_Z. It is reported that all situations studied are under pressure.

In this analysis, the mesh of the structure is refined around the zone of defect in order to have the concentrations of the stresses in a precise way at best. The convergence of the numerical calculations is obtained with difficulty according to the mesh architecture because of the small dimension of the micro-cavity. The behavior of FGM was presented using C3D8R solid elements. The number of elements used in the structure is 57970 elements for $R_{ex} / R_{in} = 1.1$, of 93954 elements for $R_{ex} / R_{in} = 1.2$ and of 49464 elements for $R_{ex} / R_{in} = 1.3$ Fig.5 shows the detail of the mesh used for the calculations.

Because of these numerous advantages, the typical gradation of FGMs in tubular systems is widely used; it becomes important to study their behavior elasto-plastic in the presence of defects under internal pressure. These defects by their location, combine both effects the location itself and the gradation of FGM; hence, the main problem in our work is to identify the effect of default in different cases. Our study is conducted by three locations following the thickness (Fig.5). The quality defect is a void which always remains trapped in the thickness. This numerical computation modality gave us the reliable advantage of creating defects in complex geometrical and loading situations without having a problem of convergence.
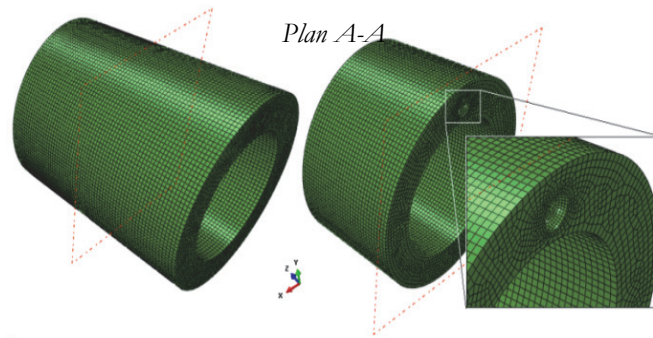
Plan A-A
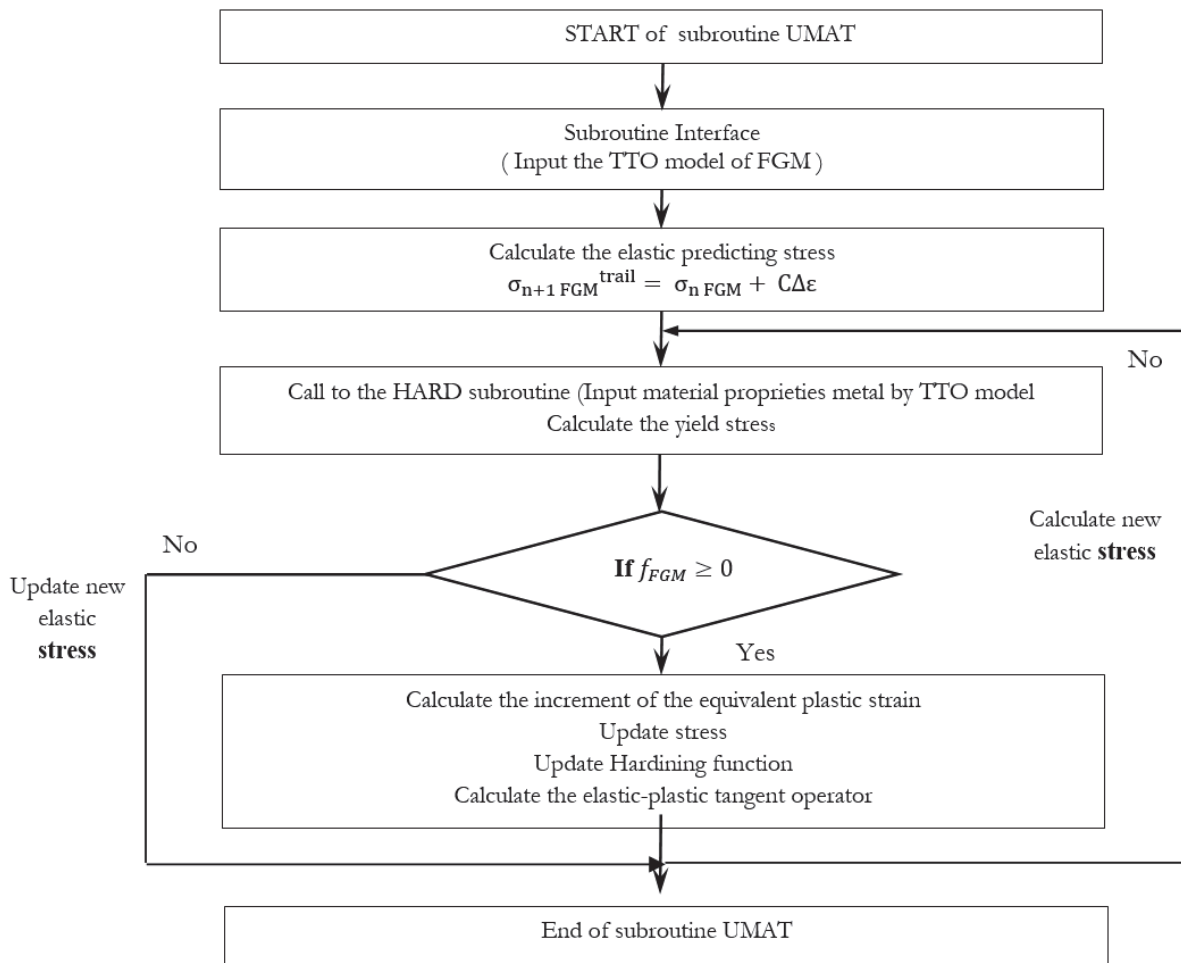
Figure 5: Details of the mesh around the cavity.

Figure 6: Presentation of the algorithm for the integration of stresses in the FGM (UMAT and HARD).

NUMERICAL IMPLEMENTATION OF THE MODEL

I n Fig.6, we have presented the numerical model used in this study as an algorithm for the UMAT technique which shows all the key steps structured and dependent on each other. These steps are necessary for the modeling of a structure. The elastoplastic behavior of the structure is used by two subroutines UMAT and HARD introduce into the calculation code ABAQUS. The equations as well as the conditions presented in the algorithm are well detailed in the previous study sections and which summarize the elastic corrections, localized plasticization of our studied FGM structure.

RESULTS AND ANALYSIS

Model validation

F or the reliability of our results, the present method is compared with the numerical results obtained by the work of Kalali and al [44] by taking into account the dimensions of the normalized model under the effect of internal pressure and by taking a distribution of the following mechanical properties the thickness of the cylinder for an exponent of the power law n = 2 and 100% ceramic (f_0= 1). The results obtained represent a very good agreement with those of Kelali et al [44] (Fig. 7).

We notice that the current solution is closer to the numerical solution proposed by Kalali and al [44]. This is mainly due to the different numerical analysis methods used in the simulations. The analysis of sensitivity to the mesh and cde onvergence of the results for the structure in three demensions led us to carry out three analyzes using elements C3D8 and C3D8R and 1000 increments of deflection / time. The elements of C3D8R have been shown to have excellent accuracy and moderate mesh dependence (Fig. 7). The aim of developing the C3D8R elements was to increase the efficiency of calculations without losing precision. The C3D8R-type mesh sensitivity was measured until further improvement in the mesh caused stability in the determination of the Von Mises stress in the FGM plate.

The effect of the mesh element density presented in Fig. 7 has shown a strong link between the numerical analysis and that of the experimental one and presents a good validation with the work of Kalali and al [44]. Note that when it comes to a large percentage of ceramic (outer face of the cylinder), the two results are much closer compared to that of the interior where the percentage of plasticity is important (presence of metal) . In fact, the plastic behavior of the metal inside the cylinder displays stresses conditioned by the plasticity criterion introduced in the calculation. This is a better way to select a good selection of mesh elements with an appropriate density. For our analysis the choice was on the elements of C3D8R with a density of 40,000 elements in the structure. Which brings us back to the end of concluding that our numerical approach with the parameters introduced is reliable.
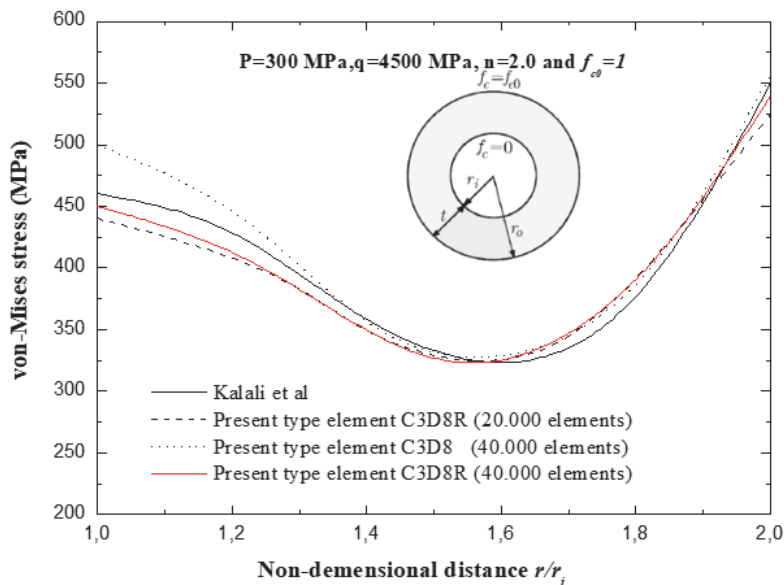

Figure 7: Von Mises stress along the thickness in the FGM cylindrical vessel subjected to internal pressure (properties listed in Tab. 1).

Effect of volume fraction exponent "n"

Fig.8 shows the variation of the different stresses (radial, circumferential, and axial for different values of the volume fraction exponent "n" for a cylinder radius ratio R_ex/R_in =1.1. Note that we set the same conditions in percentage of ceramic and metal in the ends of the cylinder thickness of 15% metal in the interior (85% ceramic) and 100% metal in the exterior under 100 MPa pressure. Radial, circumferential, and axial stresses were evaluated under radial gradation of the ceramic into the metal from the inside to the outside.

The radial stresses are greater from the inside to the outside and decrease with increasing value of the gradation exponent "n". This means that if the structure is ceramic rich, the compressive stresses are low. Similarly, the effect of the exponent "n" of the gradation has a great impact on the tangential stresses, which occur with large values compared to those of the radial and axial.
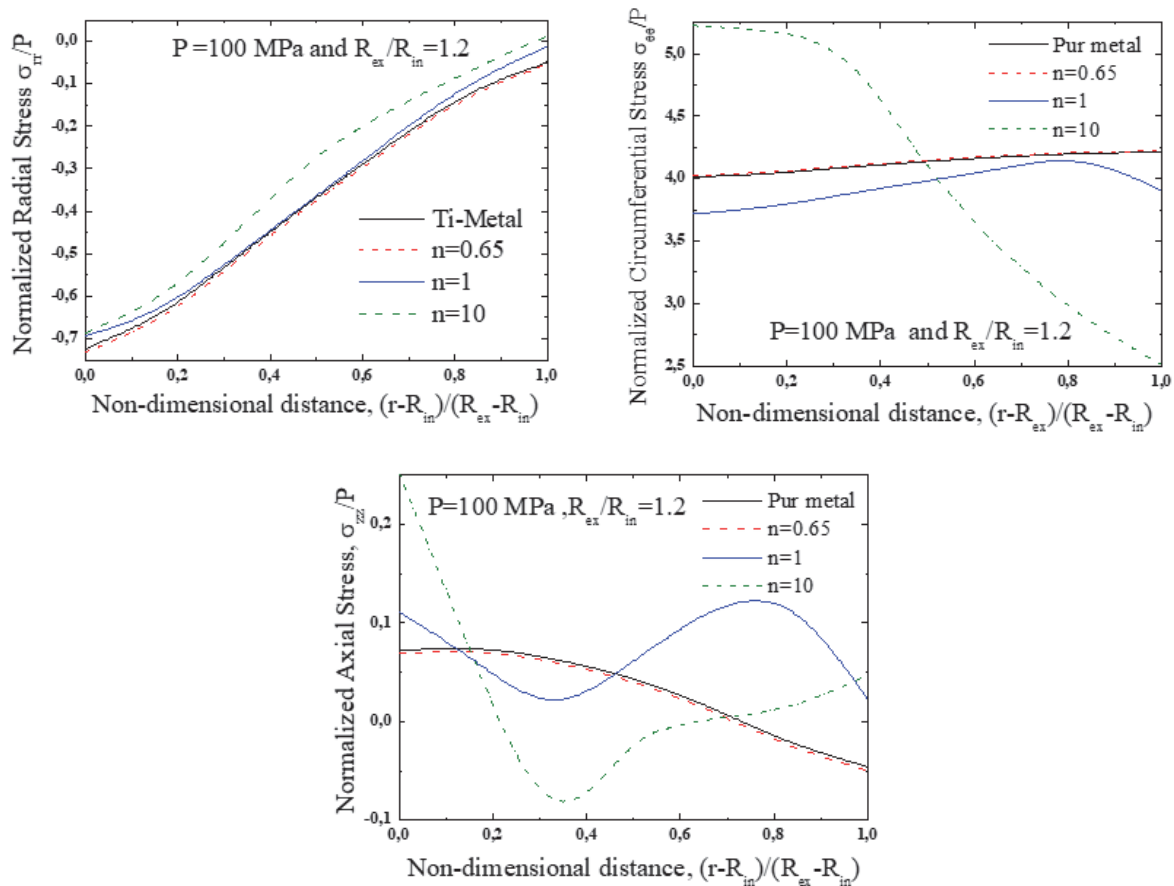

Figure 8: The variation of radial, circumferential and axial of stress according to the thickness of FGM pipe (with ratio of diameter kept constant $\left(R_{ex} / R_{in} \right) = 1.2$ and n variable).

Important values are noted for "n = 1". The axial stresses clearly marked the effect of the gradation, for the exponent n=1 the axial stresses according to the thickness are all of tension by cons they are of tension and compression for the other values of "n". We also note that when the structure is rich in ceramic, the stresses are important from the inside.

Effect of thickness under gradation

Under an internal pressure of 100 MPa and under a gradation exponent of $n = 0.65$, local plasticity occurred in some situations. Fig.9 shows the evaluation of the stresses according to the thickness of the cylinder under the effect of both the thickness and the graduation. The collection of these results from the inside to the outside has been made in the middle of the length of the cylinder so that we can ascertain that they come from the pure effect of the internal pressure.

Fig.9 shows that the radial or compressive stresses according to the thickness are more important from the outside, 100% metal inwards 85% ceramic. According to the thickness of the cylinder, the variation of the stresses has been done by effect of stiffness of the thickness and that of the graduation. Circumferential stress recorded higher values than radial and

axial stresses. More particularly for small thicknesses, these stresses are constant as a function of thickness, except that they decrease towards the outside for larger thicknesses where the effect of the gradation appears slightly. The longitudinal or axial stresses vary from the inside to the outside depending on the thickness by compressive stresses towards tensile stress. If the thickness of the cylinder is important, the presence of ceramic is dominant and therefore more rigidity, which leads to a reduction in the values of the axial stresses.
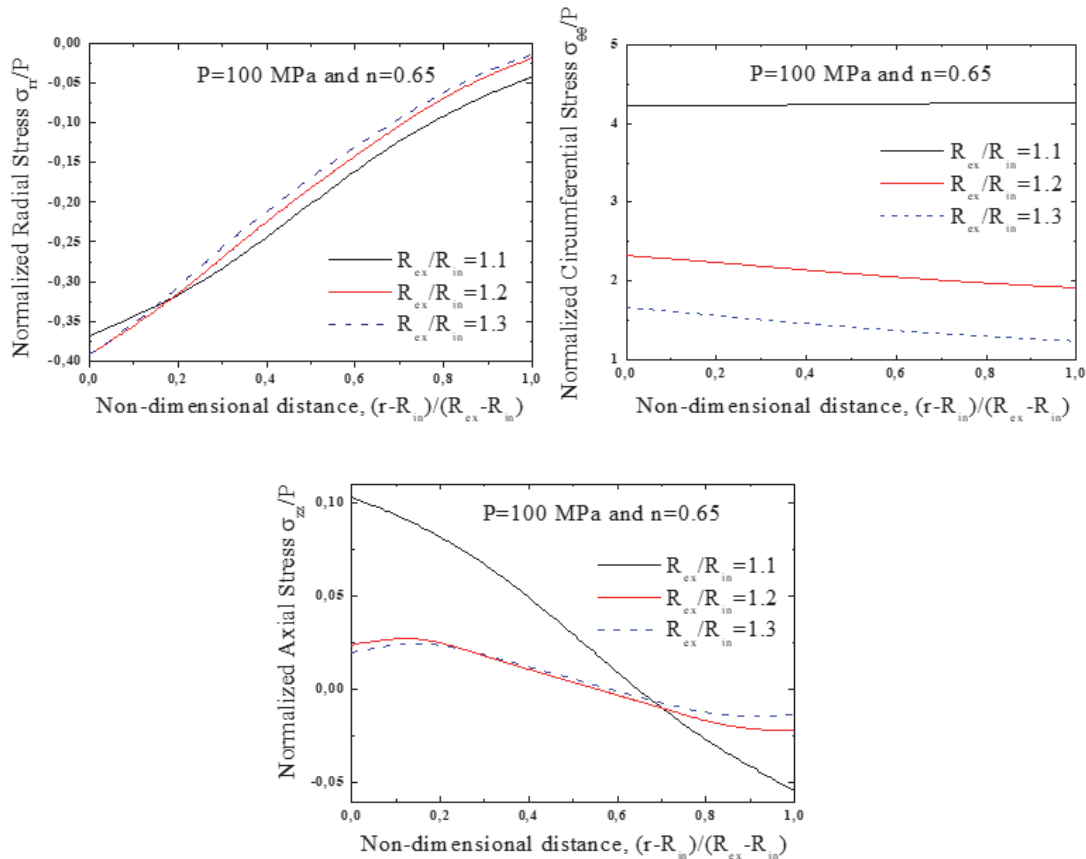
Figure 9: The variation of radial, circumferential and axial of stress according to the thickness of FGM pipe (with ratio of diameter $\left(R_{ex} / R_{in} \right)$ variable and n kept constant=0.65)

Effect of the defect location under the gradation
Radial, circumferential and axial stresses are taken according to the thickness near to the defect, where the maximum values are presented. To better compare the effect of the three locations of the defect in the FGM, a stress distribution without defects was introduced; that of the FGM and that of the pure metal because the metal is the base of the FGM (15% of the interior and 100% of the outside).
The presence and location of defects in Fig.10 shows clearly their effect on the level and distribution of radial stresses. The defect to be localized is increased by the stresses in its zone and will be more important where the defect approaches towards the end of the thickness. When the defect appears in a rigid zone or rich in ceramic, the compressive stresses will be important, and the more it moves away to the outside, the more important it is also. The defect in the middle marks a slight decrease in compressive stresses along the thickness near the defect.
The circumferential stresses presented in Fig.11 recorded much larger values than those of the radial and axial stresses. However, they are always raised towards the outside of the cylinder except for the fault, which is in the middle. The defect effect represented by a peak explains the elongation of defect in the circumferential direction in elliptical form and a significant tension at these ends. Since the material is made of FGM at the base of a metal graduated with ceramic, it always marks values slightly higher than those of pure metal.
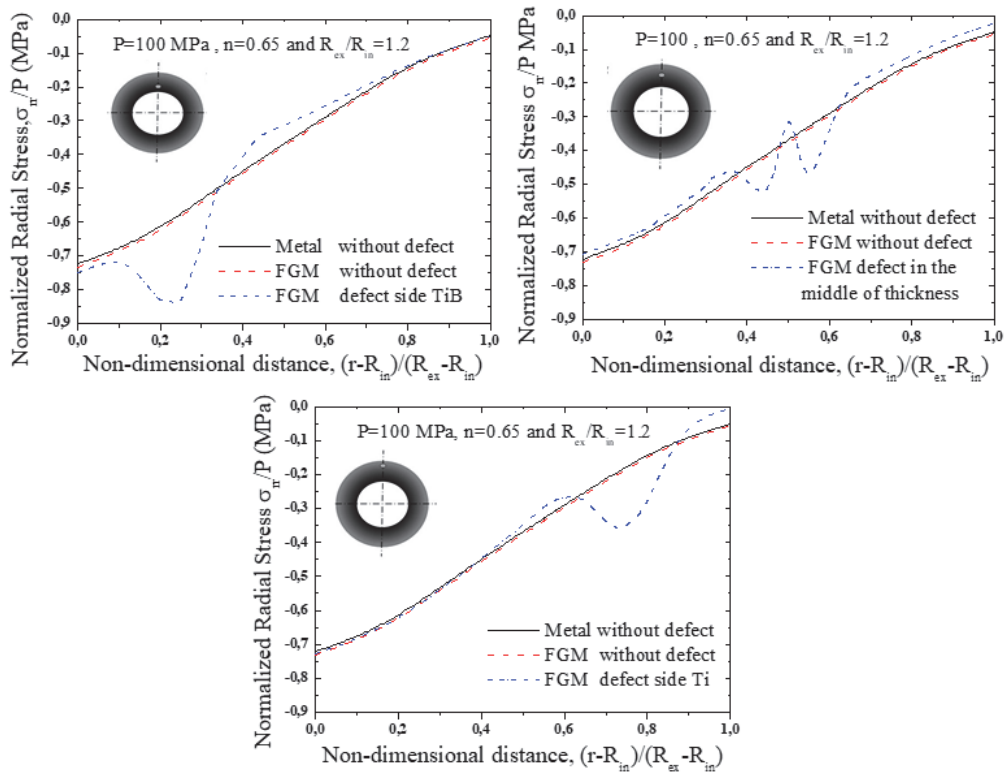
Figure 10: the variation of radial stress according to the thickness for the three positions of the defect (with ratio of radius $\left(R_{ex} / R_{in}\right)$ constant and n kept constant=0.65).

Figure 11: The variation of circumferential stress according to the thickness for the three positions of the defect (with ratio of radius $\left(R_{ex} / R_{in}\right)$ constant and n kept constant=0.65).

Figure 12: The variation of axial stress according to the thickness for the three positions of the defect (with ratio of radius (R_{ex} / R_{in}) constant and n kept constant=0.65).
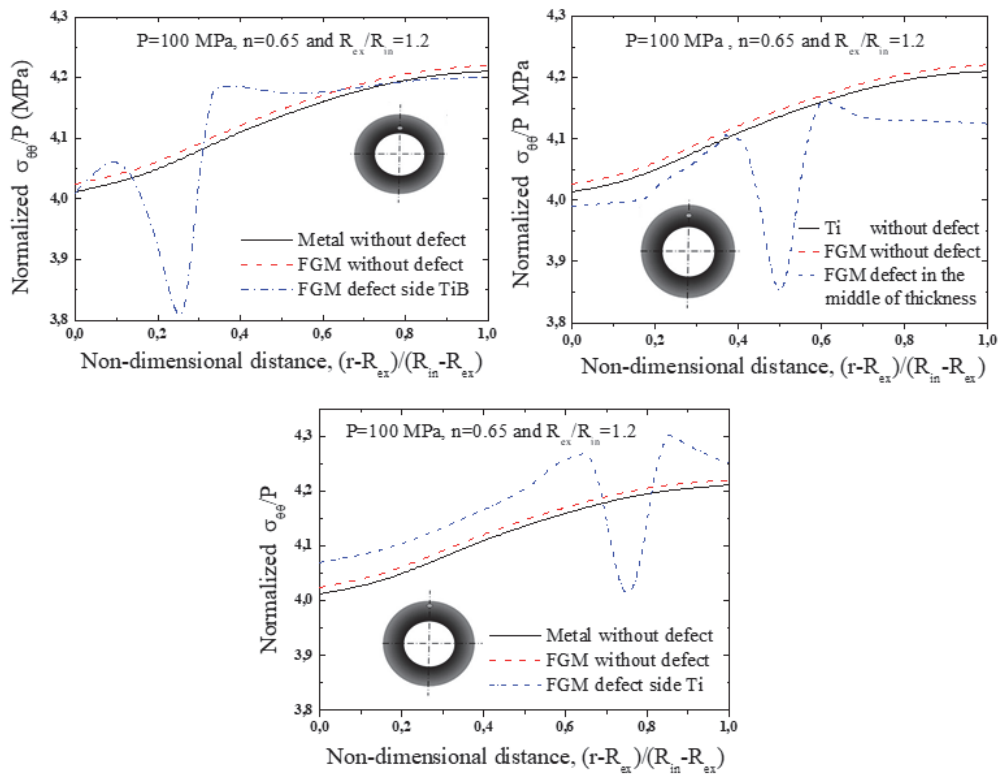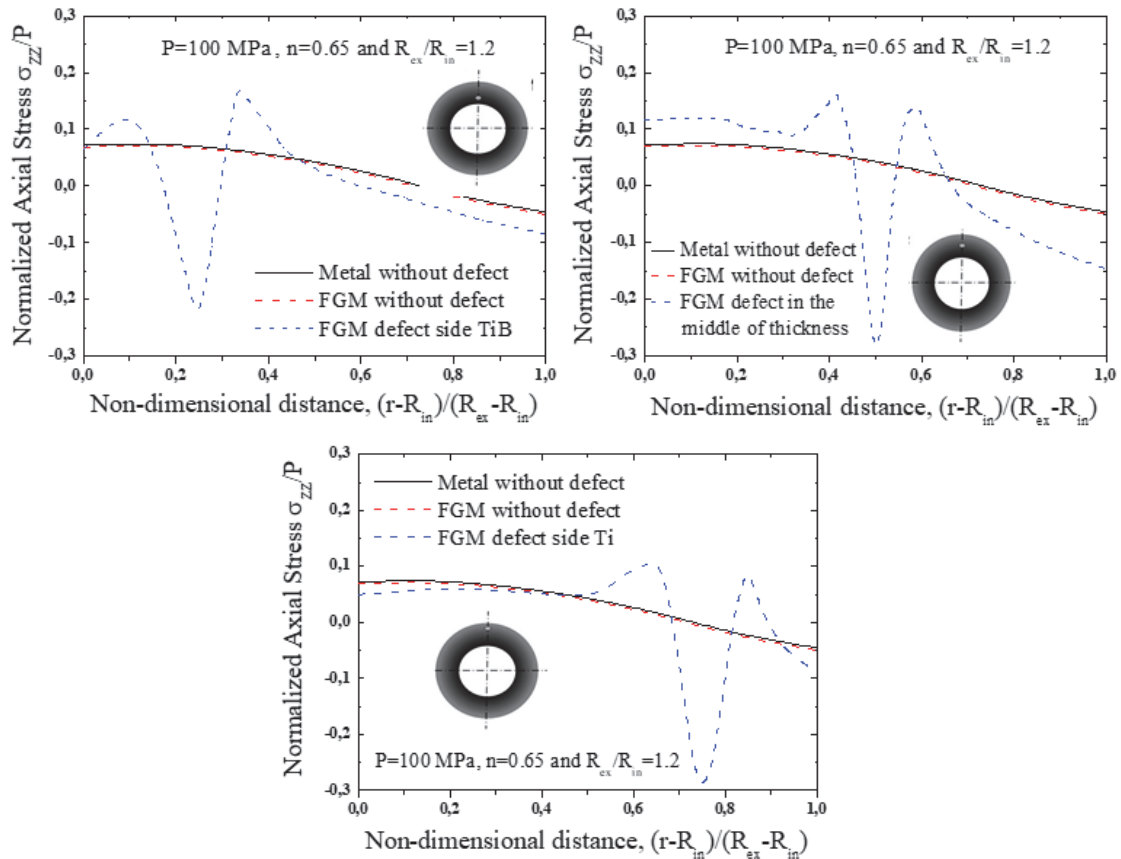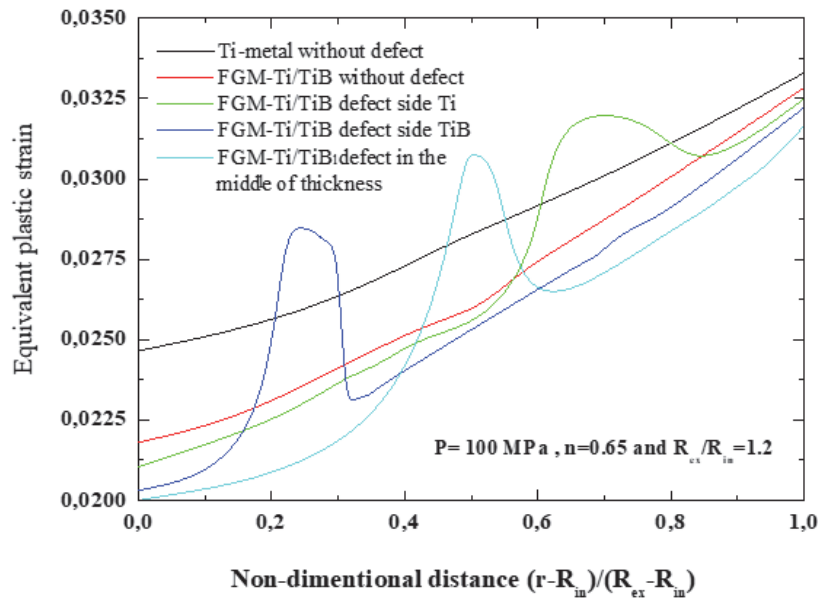

Figure 13: Equivalent plastic strain distribution in FGM cylinder (n=0.65)

In Fig.12, the axial stresses are clearly affected by the presence and location of defects that amplify the level and distribution of stresses. The peaks of the stresses explain the compression in the form of elongation in a direction slightly

oriented by the gradation effect of FGM around the defect. The latter is accompanied with a concentration in these extremities. When the defect is close to the end of the thickness, the peaks are large with a weak change at the ends, unlike the one in the middle of the thickness. It is important subsequently to analyze the plastic deformation of these structures because the behavior of the metal is plastic and which is also part of the FGM. In addition, the presence of a defect depending on the thickness of the structure did indeed cause this deformation. According to the parameters introduced into the structure such as the volume fraction, the dimension of the cylinder as well as the applied pressure, we have presented in Fig.13 the variation of the plastic deformation under the effect of the location of defect according to the thickness of the cylinder. it can be noted that the plasticity of the metal is graduated according to the thickness of the structure, it is clearly noted that in the vicinity of the defect, the plasticity displays peaks of stresses which are important in the case where the defect is close to the high percentage metal in the cylinder.

Validation of the FGM numerical model by stress-strain curves
In Fig. 14 we have presented the elastoplastic behavior of the FGM for our model. The purely elastic behavior of the ceramic TiB and that of the metal Ti, and by using the law of homogenization that of TTO, we determined the elastoplastic behavior of the graduated FGM at different volume fraction and under the effect of different situations, without and with presence of defects in different locations; close to ceramic, close to metal, and in the middle of the cylinder thickness.
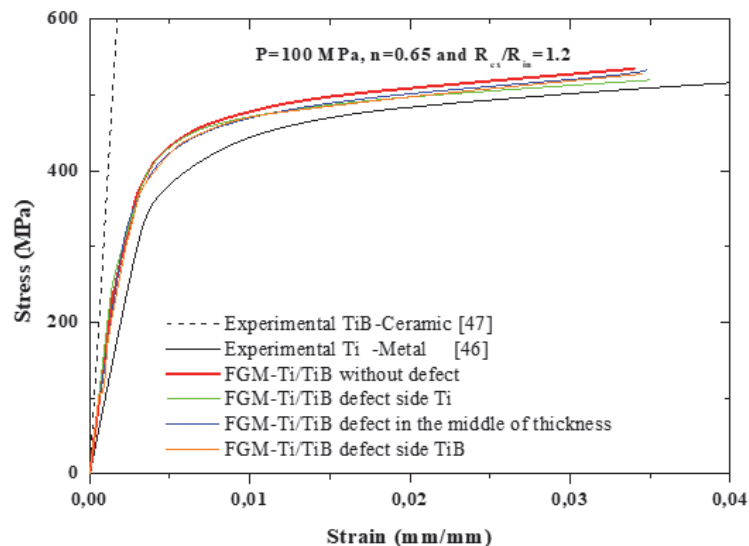

Figure 14: The true stress-strain curve of FGM Ti/TiB for n=0.65 and curve of Ti and TiB.

We clearly notice in Fig. 14 for a volume fraction n = 0.65 that is to say the FGM is rich in metal, that the presence of the defect as well as its location according to the thickness considerably influences the value of the various stresses in the cylinder.Indeed, the stress-strain response of structure with the presence of defects displays relatively lower values, especially when it is a defect close to the metal side. this result clearly explains that the presence of a defect is a lack of materials in the structure which absorbs the stresses by plastic deformation much more.
This Fig.15 shows the radial, tangential and axial stresses for different locations of the defect according to the thickness of the FGM pipe. It also shows the location of higher and lower stress concentration.

CONCLUSION

A study based on finite element analysis was carried out to understand the influence of the position of a spherical cavity in a tubular FGM structure of type TiB/Ti subjected only to internal pressure. The analysis takes into account the elastoplastic behavior of the cylinder by introducing the mechanical properties of the two metals (ceramic and metal) in the calculation code Abaqus. The UMAT analysis technique was used and compared with the literature for the Von Mises stress and with the experimental stress-strain curve of the structure in order to validate the numerical model where we can note a good agreement.

- We were able to validate our numerical model following a study of sensitivity of mesh elements and we chose the element of type C3DR8 the most used and effective for the structures in FGM.
- The UMAT technique presents a good efficiency in the modeling of a tubular structure in FGMs. The results obtained allowed us to evaluate the different parameters influencing the distribution of radial, tangential and axial stresses of the structure.
- The technique of modeling the behavior of a FGM structure by UMAT in abaqus has shown its effectiveness against the experimental and it could be extended for more application especially in the modeling of cancellous bones.
- The TTO model has proven to be effective in determining the behavioral parameters of FGMs by including the plasticity of the metal and using solid elements of the C3DR8 type.
- For a cylinder under pressure, depending on its thickness, the radial, circumferential and axial stresses are tension-compression and shear stresses respectively. The tubular structure undergoes more circumferential stresses in tension than by the other stresses.
- The gradation exponent "n" plays an important role on the stress levels and distribution, the more concentrated the FGM is in a stiff material the stiffer it becomes and the more the structure as a function of stress type gives large values.
- If the thickness of the cylinder increases, the FGM structure becomes more and more rigid. This rigidity is amplified by the presence of the ceramic material which then gives higher stresses.
- In the FGM, if the micro-cavity is lodged towards the graduated rigid element, the stress concentration is important.
- A peak of overstress appears at the level of the cavity where its value depends on the position of the cavity in relation to the metal or ceramic
- The position of the defect according to the thickness of the metal towards the ceramic generates important values of the circumferential stresses which will cause a deterioration of the structure for more pressure. In addition, the presence of a void at the different locations can generate low or high stresses depending on the presence of ceramic or metal.
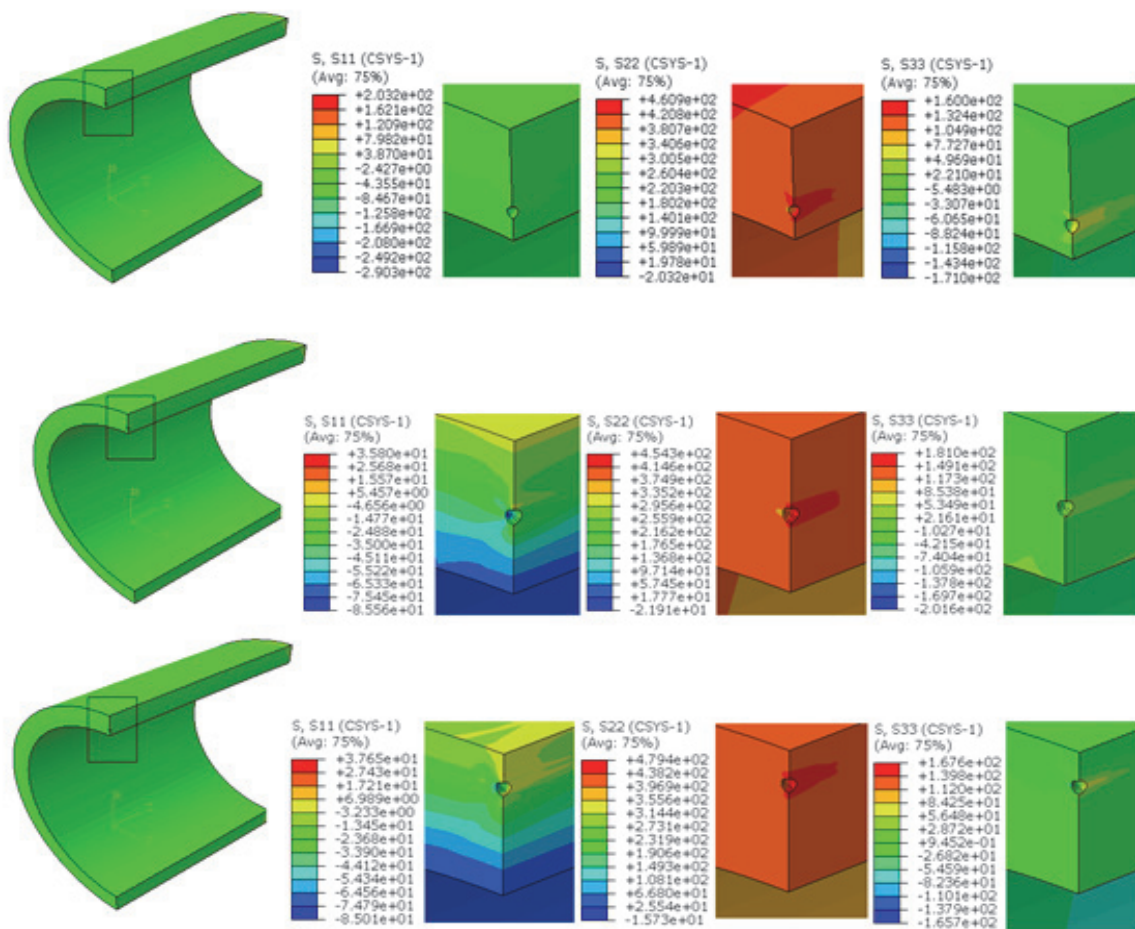

Figure 15: Presentation of the stresses level around cylinder thickness for the three positions of the defect.

REFERENCES

[1] Hirai, T. (1991). Fabrication and Properties of Functionally Gradient Materials, Journal STAGE., 99 (1154), pp. 1002-1013. DOI: 10.2109/jcersj.99.1002.

[2] Watanabe, Y., Inaguma, Y. and Sato, H. (2009). A novel fabrication method for functionally graded materials under centrifugal force: the centrifugal mixed-powder method, Materials., 2(4), pp.2510–2525. DOI:10.3390/ma2042510.

[3] Mehdi, G. and Hamed, G. (2014). Displacements and stresses in pressurized thick FGM cylinders with exponentially varying properties based on FSDT, Journal Structural Engineering and Mechanics., 51(6), pp.939-953. DOI:10.12989/sem.2014.51.6.939.

[4] Kerimcan, C., Durmus, Y. and Ibrahim, K.(2016). A unified method for stresses in FGM sphere with exponentially-varying properties, Structural Engineering and Mechanics., 57(5), pp.823-835. DOI:10.12989/sem. 2016.57.5.823.

[5] Abdelhakim, K., Khalil, B., Abdelouahed, T. and El Abbes, B.(2014). Nonlinear cylindrical bending analysis of E-fgm plates with variable thickness, Steel and Composite Structures., 16(4), pp.339-356. DOI: 10.12989/ scs.2014.16.4.339.

[6] Chih-Ping,W. and Yan-Cheng, L. (2016). A state space meshless method for the 3D analysis of fgm axisymmetric circularplates, Steel and Composite Structures., 22(1), pp.161-182. DOI:10.12989/scs.2016.22.1.161.

[7] Bich, D.H., Ninh, D.G. and Tran, I.T. (2016).Non-linear buckling analysis of FGM toroidal shell segments filled inside by an elastic medium under external pressure loads including temperature effects, Composites Part B. Engineering., 87, pp.75-91. DOI:10.1016/j.compositesb.2015.10.021.

[8] Kordkheili, S.A.H., Naghdabadi, R. (2007). Thermoelastic analysis of a functionally graded rotating disk, Composite Structures.,79(4), pp. 508–516. DOI:10.1016/j.compstruct.2006.02.010.

[9] Safari, A., Tahani, M ., Hosseini.(2011). Two-dimensional dynamic analysis of thermal stresses in a finite-length FG thick hollow cylinder subjected to thermal shock loading using an analytical method, Acta. Mech., 220(1-4), pp. 299-314. DOI:10.1007/s00707-011-0478-y.

[10] Sharma, S., S, Yadav., R, Sharma. (2017). Thermal Creep Analysis of Functionally Graded Thick- Walled Cylinder Subjected to Torsion and Internal and External Pressure, Journal of Solid Mechanics., 09(2), pp. 89-98. DOI: 10.22059/JCAMECH.2017.233633.143.

[11] You, L.H., Zhang, J.J., You, X.Y. (2004). Elastic analysis of internally pressurized thick-walled spherical pressure vessels of functionally graded materials, International Journal of Pressure Vessels and Piping., 82(5), pp.347–354. DOI:10.1016/j.ijpvp.2004.11.001.

[12] Foroutan, M., R, Moradi. and R, Sotoodeh-Bahreini. (2011). Static analysis of FGM cylinders by a mesh-free method, Steel and Composite Structures., 12(1), pp. 1-11. DOI:10.12989/scs.2011.12.1.001.

[13] Gharooni, H., Ghannad, M., and Nejad, M.Z. (2016). Thermo-Elastic Analysis of Clamped-Clamped Thick FGM Cylinders by Using Third-Order Shear Deformation Theory, Latin American Journal of Solids and Structures., 13(4), pp. 750-774. DOI:10.1590/1679-78252254.

[14] Ahmet, N.E. (2007). Stresses in FGM pressure tubes under non-uniform temperature distribution, Structural Engineering and Mechanics., 26(4), pp. 393-408. DOI:10.12989/sem.2007.26.4.393.

[15] Ghannad et al. (2012). Elastic analysis of exponential FGM disks subjected to internal and external pressure, Open Engineering., 03(3), pp. 459-465. DOI:10.2478/s13531-013-0110-0.

[16] Chen, Y.Z. (2018). Transfer matrix method for solution of FGMs thick-walled cylinder with arbitrary inhomogeneous elastic response, Smart Structures and Systems., 21(4), pp. 469-477. DOI: 10.12989/sss.2018.21.4.46.

[17] Bayat, Y., Ghannad, M. and Torabi, H. (2012). Analytical and numerical analysis for the FGM thick sphere under combined pressure and temperature loading, Arch Appl Mech., 82, pp. 229–242. DOI:10.1007/s00419-011-0552-x.

[18] Carrera, E., Brischetto, S. and Robaldo, A. (2008). Variable Kinematic Model for the Analysis of Functionally Graded Material plates, AIAA Journal., 46(1), pp. 194–203. DOI:10.2514/1.32490.

[19] Cinefra, M., Carrera, E. and Brischetto, S. (2010). Analyse thermomécanique des coquilles fonctionnellement calibrées, Journal of Thermal Stresses., 33(10), pp. 942–963. DOI :10.1080/01495739.2010.482379.

[20] Bachir, B., Mohammed, S., Ah, H. and Abdelouahed, T. (2013). Thermomechanical bending response of fgm thick plates resting on Winkler-Pasternak elastic foundations, Steel and Composite Structures., 14(1), pp. 85-104. DOI: 10.12989/scs.2013.14.1.085.

[21] Otbi, B., Khalil, B., Abdelouahed, T. and El Abbes, A.B. (2015). Numerical analysis of fgm plates with variable thickness subjected to thermal buckling, Steel and Composite Structures., 19 (3), pp. 679-695.

DOI: 10.12989/scs.2015.19.3.679.

[22] Merbouha, B., Kouider, H.B., Ahmed, B. and Abdelouahed, T. (2016). Thermal post-buckling behavior of imperfect temperature-dependent sandwich FGM plates resting on Pasternak elastic foundation, Steel and Composite Structures, 22 (1), pp. 91-112. DOI: 10.12989/scs.2016.22.1.091.

[23] Abdelhakim, K., Khalil, B., Abdelouahed, T and El Abbes, A.B. (2014). Nonlinear cylindrical bending analysis of E-FGM plates with variable thickness, Steel and Composite Structures, 16(4), pp. 339-356. DOI:10.12989/scs.2014.16.4.339.

[24] Kerimcan, C., Durmus, Y. and Ibrahim, K. (2016). A unified method for stresses in FGM sphere with exponentially-varying properties, Structural Engineering and Mechanics.,57(5), pp. 823-835. DOI:10.12989/sem. 2016.57.5.823.

[25] Sharma, S., Yadav, S., Sharma, R. (2017). Thermal creep analysis of functionally graded thick-walled cylinder subjected to torsion and internal and external pressure, Journal of Solid Mechanics., 9(2) , pp. 302–318.

[26] Wang, Z.W., Zhang, Q., Xia, L.Z., Wu, J.T., Liu, P.Q. (2015). Stress Analysis and Parameter Optimization of an FGM Pressure Vessel Subjected to Thermo-Mechanical Loadings, Procedia, Eng., 130, pp. 374–389. DOI: 10.1016/ j.proeng .2015.12.230.

[27] Praveen, G. N., Chin, C.D. and Reddy, J.N. (1999). Thermoelastic Analysis of Functionally Graded Ceramic-Metal Cylinder, Journal of Engineering Mechanics., 125(11), pp. 125:11. DOI: 10.1061/(ASCE)0733-9399.

[28] Horgan, C.O., Chan, A.M. (1999). The Pressurized Hollow Cylinder or Disk Problem for Functionally Graded Isotropic Linearly Elastic Materials, Journal of Elasticity., 55(1), pp. 43–59. DOI:10.1023/A:1007625401963.

[29] Figueiredo, F., Borges, L. and Rochinha, F. (2008). Elasto-plastic stress analysis of thick-walled FGM pipes, AIP Conference Proceedings., 973(1), pp. 147. DOI:10.1063/1.2896766.

[30] Trabelsi, S., Frikha, A., Zghal, S. and Dammak, F. (2018). Thermal postbuckling analysis of functionally graded material structures using a modified FSDT, Int J Mech Sci., 144, pp. 74-89. DOI:10.1016/j.ijmecsci.2018.05.033.

[31] Kar, V.R., Panda, S. (2015). Large deformation bending analysis of functionally graded spherical shell using FEM, Struct. Eng. Mech., 53(4), pp. 661–679. DOI:10.12989/sem.2015.53.4.661.

[32] Kar, V.R., Panda, SK. (2016). Post-buckling behaviour of shear deformable functionally graded curved shell panel under edge compression, Int.J.Mech.Sci., 115-116, pp. 318–324. DOI: 10.1016/j.ijmecsci.2016.07.014.

[33] Hanen, J., Jamel, M., Mondher, W. and Fakhreddine, D. (2018). An extended finite element method for modeling elastoplastic FGM plate-shell type structures, Structural Engineering and Mechanics, 68(3), pp. 299-312. DOI: 10.12989/sem.2018.68.3.299.

[34] Amir, T., Kalali, Saied., Hadidi, Moud. and Behrooz, Hassani. (2016). Elasto-Plastic Stress Analysis in Rotating Disks and Pressure Vessels Made of Functionally Graded Materials, Latin American Journal of Solids and Structures., 13 (5). DOI:10.1590/1679-78252420.

[35] Kutlu, D. (2015). Vibration analysis of functionally graded material (fgm) grid systems, Steel and Composite Structures., 18(2), pp.395-408. DOI:10.12989/scs.2015.18.2.395.

[36] Hadji, L., Daouadji, T.H., Tounsi, A. and Bedia, E. (2014). A higher order shear deformation theory for static and free vibration of fgm beam, Steel and Composite Structures., 16(5), pp. 507-519, DOI:10.12989/scs.2014.16.5.507.

[37] Khalid, M., Abdelkrim, B. and Youcef, B. (2018). Three dimensional finite elements modeling of FGM plate bending using UMAT, Structural Engineering and Mechanics., 66(4), pp. 487-494. DOI:10.12989/sem .2018.66.4.487.

[38] Benferhat, R., Hassaine, T., Hadji, L, and Mansour, M. S. (2016). Static analysis of the FGM plate with porosities, Steel and Composite Structures., 21(1), pp. 123-136. DOI:10.12989/scs.2016.21.1.123 .

[39] Benferhat, R., Tahar, H. Daouadji. and Rabahi, A. (2019). Effect of porosity in interfacial stress analysis of perfect FGM beams reinforced with a porous functionally graded materials plate, Structural Engineering and Mechanics., 72(3), pp. 293-304. DOI:10.12989/sem.2019.72.3.293.

[40] Nguyen, N.V., Nguyen, H.X., Lee, S. and Nguyen-Xuan, H. (2018). Geometrically nonlinear polygonal finite element analysis of functionally graded porous plates, Adv. Eng. Softw., 126, pp. 110–126. DOI:10.1016/j.advengsoft.2018.11 .005.

[41] Jae-Chul, L. (2015). Sintering Behavior and Material Properties of Nickel/Alumina Functionally Graded Materials Fabricated by Pressureless Sintering Method, School of Mechanical and Aerospace Engineering, China.

[42] Bekki, H., Benferhat, R. and Tahar, H. D. (2019). Influence of the distribution shape of porosity on the bending FGM new plate model resting on elastic foundations, Structural Engineering and Mechanics., 72(1), pp. 61-70. DOI:10.12989/sem.2019.72.1.061.

[43] Carpenter, D., Liang, W., Paulino, G. H., Gibeling, J. C. and Munir, Z. A. (1999). Fracture testing and analysis of a layered functionally graded Ti/TiB beam in 3-point bending, Materials Science Forum., pp. 837–842. DOI: 10.4028/www.scientific.net/MSF.308-311.837.

[44] Kalali, A.T., Hassani, H. and Saied, H. (2016). Elastic-plastic analysis of pressure vessels and rotating disks made of functionally graded materials Using the isogeometric approach, Journal of Theoretical and applied Mechanics., 54(1), pp. 113-125. DOI:10.15632 / jtam-pl.54.1.113.

[45] Panda, K.B., Chandran, K.S. (2003). Titanium-titanium boride (Ti-TiB) functionally graded materials through reaction sintering: Synthesis, microstructure, and properties, Metall. Mater. Trans., 34, pp. 1993–2003. DOI:10.1007/s11661-003-0164-3.

[46] Jin, ZH., Paulino, GH. and Dodds, RH. (2003). Cohesive fracture modeling of elastic–plastic crack growth in functionally graded materials, Engineering Fracture Mechanics.., 70(14), pp. 1885–1912. DOI:10.1016/S0013-7944 (03) 00130-9.

[47] Houari, A., Mokhtari, M., Bouchikhi, A.S., Polat, A. and Madani, K. (2021). Using finite element analysis to predict the damage in FGM-3D notched plate under tensile load; Different geometric concept, Engineering Structures., 237, 112160. DOI:10.1016/j.engstruct.2021.112160